BER the international journal of bridge engineering management and research

Clustering-Based Framework for Multi-Sensor Data Fusion in Bridge Deck Condition Assessment

Ibukunoluwa Grace Tella[1,*]; Eyosias Beneberu[2]; and Nur Yazdani[3]

Submitted: 08 August 2025 **Accepted:** 15 September 2025 **Publication date:** 10 October 2025

DOI: 10.70465/ber.v2i4.50

Abstract: Bridge deck deterioration poses a significant challenge to transportation infrastructure, resulting in costly maintenance and potential safety hazards. Traditional bridge deck assessments primarily rely on visual inspections, which can be subjective and may fail to capture subsurface defects, such as delamination, rebar corrosion, and concrete degradation. To enhance the accuracy of condition assessment, this study explores multi-sensor data fusion and clustering techniques for defect identification using ground penetrating radar and impact echo (IE). By integrating multiple non-destructive evaluation datasets, a clustering-based framework was developed to automatically categorize bridge deck conditions. K-Means, density-based spatial clustering of applications with noise (DBSCAN), Gaussian Mixture Models, and Fuzzy C-Means clustering algorithms were evaluated to determine their effectiveness in grouping similar defect patterns. The optimal number of clusters was determined using the Elbow Method, Silhouette Score, and Davies–Bouldin Index. Results indicate that DBSCAN outperforms other clustering techniques in detecting defect hotspots while effectively handling noise and spatial inconsistencies. The clustered defects are mapped spatially to visualize regions of deterioration, enabling bridge engineers to identify high-risk areas and prioritize maintenance efficiently.

Author keywords: Bridge condition assessment; non-destructive evaluation (NDE); ground penetrating radar (GPR); impact echo (IE); clustering algorithms

Introduction

Bridge decks are critical components of transportation infrastructure, yet they are among the most susceptible to deterioration. Exposure to traffic loads, environmental stressors, and material aging accelerates the formation of cracks, delamination, spalling, and corrosion of embedded rebar (Fig. 1).[1,2] Traditionally, bridge condition assessments rely on visual inspections, as reported in the National Bridge Inventory (NBI), which uses a 0–9 rating scale based on observed surface defects.[3] However, visual inspections are inherently subjective and often fail to detect subsurface deterioration before it becomes severe.[4] This limitation leads to delayed maintenance, increased repair costs, and, in extreme cases, catastrophic failure. Several studies have highlighted the limitations of visual inspections, including inconsistencies among inspectors and the inability to detect early-stage subsurface defects.[1,5] Non-destructive evaluation (NDE) technologies offer the potential to enhance the accuracy of concrete bridge deck assessment, as they enable early detection of subsurface defects, such as delamination, rebar corrosion, and concrete degradation, without causing physical damage. These noninvasive techniques facilitate more effective maintenance planning and reduce long-term repair costs.[1,6,7,8,9,10,11]

The FHWA and various Departments of Transportations (DOTs) have increasingly adopted NDE technologies to improve traditional bridge evaluation.[6] Among the various NDE methods, ground penetrating radar (GPR) and impact echo (IE) have been widely adopted for bridge deck condition assessment.[1,12,13]

GPR transmits electromagnetic waves into concrete substrates and records the reflected signals to assess internal conditions, such as rebar cover, moisture intrusion, and material quality.[5,14] The system, often mounted on a three-wheel cart or truck (Fig. 2), enables rapid scanning of bridge deck areas. Reflected signals are displayed as radargrams, which aid in identifying subsurface anomalies. Hyperbolic patterns in the radargram indicate the presence of embedded features such as rebars, while the A-scan waveform, a one-dimensional plot of signal amplitude versus time or depth at a single point, highlights amplitude changes with depth (Fig. 3).

*Corresponding Author: Ibukunoluwa Grace Tella. Email: igo8917@mavs.uta.edu

[1]PhD Candidate, Department of Civil Engineering, The University of Texas at Arlington

[2]Associate Professor of Practice, Department of Civil Engineering, The University of Texas at Arlington

[3]Dr. Tseng Huang Endowed Professor, Department of Civil Engineering, The University of Texas at Arlington

Discussion period open till six months from the publication date. Please submit separate discussion for each individual paper. This paper is a part of the Vol. 2 of the International Journal of Bridge Engineering, Management and Research (BER), ISSN 3065-0569.

Figure 1. Bridge deck deterioration

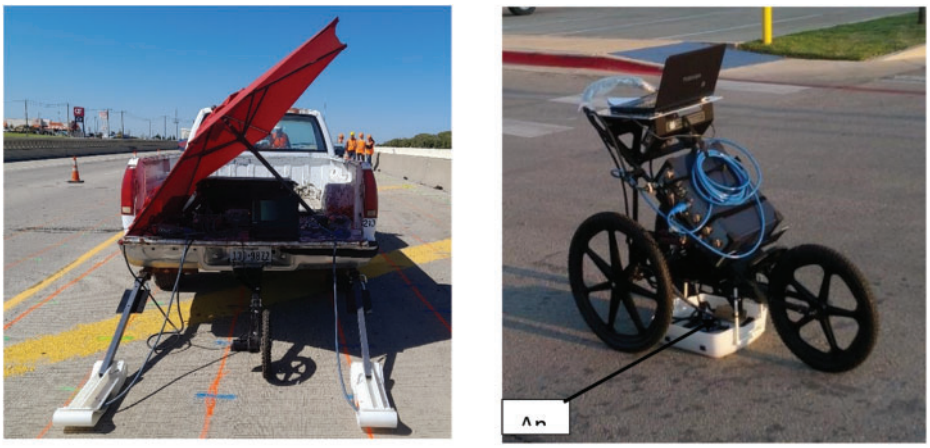

(a) (b)

Figure 2. GPR system. (a) Truck-mounted GPR and (b) Three-wheel cart-mounted GPR

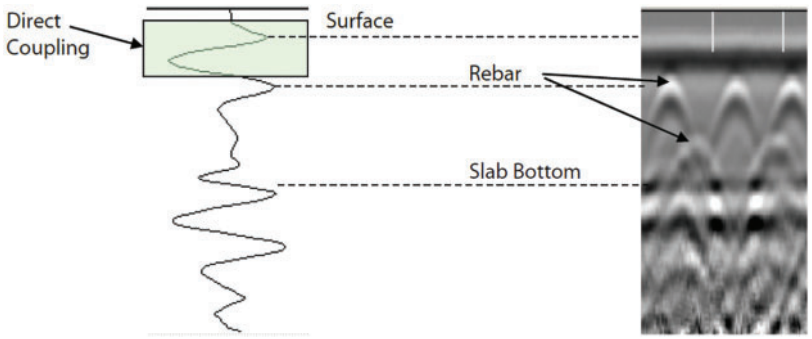

Figure 3. Typical GPR radargrams for bridge deck analysis[15]

Several studies have demonstrated the effectiveness of GPR in bridge deck evaluation. Hasan and Yazdani[16] investigated a Texas bridge deck using a 2.6 GHz antenna to detect variations in rebar cover depth. The study revealed that nearly 48% of the deck had inadequate cover. Hugenschmidt[17] conducted GPR scans on multiple bridges using a 1.2 GHz antenna and successfully identified asphalt pavement thickness variations and rebar cover inconsistencies with an average error of 6 mm when compared to core samples. These findings highlight the precision and reliability of GPR in noninvasive bridge deck assessment. However, it has limitations, including signal attenuation in moisture-rich environments and reduced effectiveness in detecting air-filled voids or delaminations.[18]

IE is a stress-wave-based technique used to detect concrete thickness and internal defects, such as delaminations, voids, and cracks, in bridge decks. The device can be a hand-held unit or a sonic surface scanner, as shown in Fig. 4. It provides a comprehensive view of subsurface conditions through analysis of frequency response.[13] The

method involves striking the deck surface with a mechanical impactor, generating stress waves that travel through the concrete. When these waves encounter defects, they reflect to the surface at distinct frequencies, which are then captured by a sensor (Fig. 5). Analyzing the frequency spectrum reveals the presence, depth, and extent of defects. Higher frequencies indicate shallower anomalies, while lower frequencies correspond to deeper defects. IE is particularly effective at detecting early-stage deterioration caused by rebar corrosion and freeze–thaw cycles, distinguishing between intact and deteriorated concrete.[19] However, the traditional hand-held IE device can be time-consuming, as it requires point-by-point surface contact and is sensitive to surface roughness. In contrast, the sonic surface scanner–IE system enables faster, continuous deck scanning, significantly improving efficiency and minimizing traffic disruptions. La et al.[20] successfully identified delaminations across multiple bridges using IE, later confirmed through coring. By integrating IE with GPR, the study provided a comprehensive assessment of both rebar-related issues and concrete integrity. Combining these methods enhances bridge condition assessment, allowing engineers to make informed decisions for maintenance and rehabilitation.

Although both GPR and IE provide valuable insights, no single technique can comprehensively assess concrete bridge deck condition. Despite the valuable data generated by these methods, their effectiveness is often limited by the need for manual interpretation and the complexity of large datasets. Machine learning (ML) algorithms enable efficient processing of large volumes of data, minimizing human error and subjectivity in defect classification. Additionally, they provide a promising approach to automating defect detection, enhancing classification accuracy, and improving predictive modeling.

ML techniques, particularly unsupervised clustering algorithms, can provide innovative solutions for bridge deck condition assessment by categorizing defect patterns without predefined labels.[19] Clustering algorithms group similar data points, making them valuable for automated defect identification and categorization of NDE data. Unlike threshold-based methods, clustering algorithms adapt to complex data distributions, enhancing defect detection accuracy. Several recent studies have also explored the use of multi-sensor data fusion, combiningGPR and IE with unsupervised learning.[21,22,23,24] Hoxha et al.[25] developed a robotic platform that integrates GPR and IE for automated subsurface defect mapping, demonstrating the potential for combining mobility with data-driven condition assessment. Similarly, Jafari and Dorafshan[26] compared supervised and unsupervised approaches for delamination detection using IE data, highlighting the advantages of unsupervised learning in the absence of labeled datasets. Völker and Shokouhi[27]

Figure 4. IE device. (a) Sonic surface scanner–IE system and (b) Hand-Held IE system

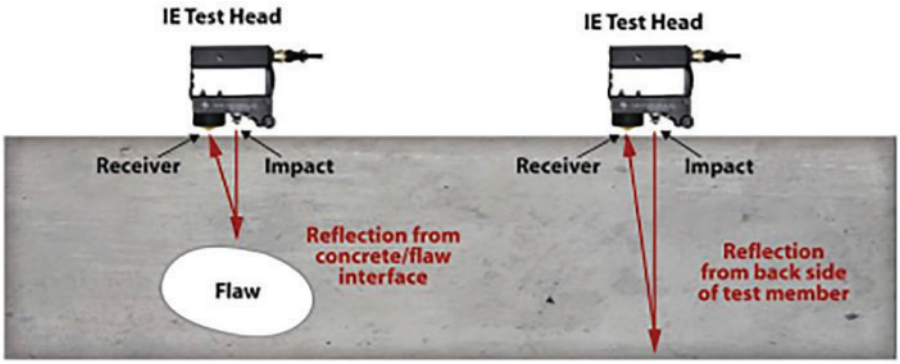

Figure 5. IE working principle

applied clustering-based fusion of IE, GPR, and ultrasound data for detecting simulated honeycombing in a concrete slab. The study demonstrated that density-based spatial clustering of applications with noise (DBSCAN) outperformed both K-Means and Fuzzy C-Means (FCMs), improving defect detectability by up to 10%. However, their study was limited to lab-scale testing on a single concrete specimen, and the transportability of their method to field-scale data remains an open question.

Various clustering techniques have been applied to bridge condition assessment, including K-means, DBSCAN, Gaussian Mixture Models (GMMs), and FCMs. K-Means, a centroid-based algorithm, assigns each data point to the nearest cluster center; however, it remains sensitive to outliers and noise.[28] DBSCAN identifies clusters based on point density, making it well-suited for detecting defect hotspots, handling irregular distributions in NDE datasets, and managing noise without needing a predefined number of clusters.[29] GMM employs probabilistic clustering with soft assignments, enabling the effective detection of overlapping defect regions and providing flexibility in modeling.[30] FCM, similar to GMM, enhances clustering by permitting data points to belong to multiple clusters, making it effective for analyzing uncertain and transitional defect zones in NDE data.[31]

Several studies have applied ML to NDE techniques, but most focus on single method clustering rather than true multi-sensor fusion. For example, Dinh and Zayed[5] developed a fuzzy logic-based approach using GPR data alone, lacking delamination insights from IE. Gagarin et al.[18] proposed a step-frequency GPR model that addresses only rebar corrosion without spatial clustering. Ibrahim et al.[19] applied fuzzy clustering to bridge deck defects, but did not integrate multiple NDE datasets. Additionally, Pedram et al.[32] used ML algorithms to analyze infrared images of reinforced concrete structures, improving corrosion defect identification. Omar and Nehdi[33] applied clustering algorithms to UAV-based infrared thermography (IRT) data, segmenting thermal images to detect delaminations without disrupting traffic.

Although these techniques enhance defect detection, challenges remain in integrating multiple large-volume NDE datasets and extracting meaningful condition patterns. Despite advancements in applying ML to NDE, most studies have focused on single-method analysis, often neglecting the integration of diverse NDE datasets needed for comprehensive defect identification. While past studies have shown the value of combining sensors and ML, most have been limited to lab environments, robotic setups, or isolated structural elements. The current research addresses this knowledge gap by developing a clustering-based multi-sensor data fusion framework that combines GPR and IE data to provide an automated and objective assessment of bridge deck condition. The proposed methodology was applied to eight full-scale bridges with diverse deck types, each with distinct construction techniques and deterioration patterns, demonstrating the practical scalability and real-world applicability of unsupervised learning in bridge deck evaluation. Building upon previous works,[5,19,32,33] this study integrates GPR and IE data within a clustering-based condition assessment model, offering a highly comprehensive view of bridge deck deterioration. This will consequently enhance accuracy, reliability, and efficiency in bridge infrastructure evaluation. The combination of GPR, IE, and ML-based clustering provides a robust approach to bridge monitoring, supporting improved maintenance and rehabilitation planning.

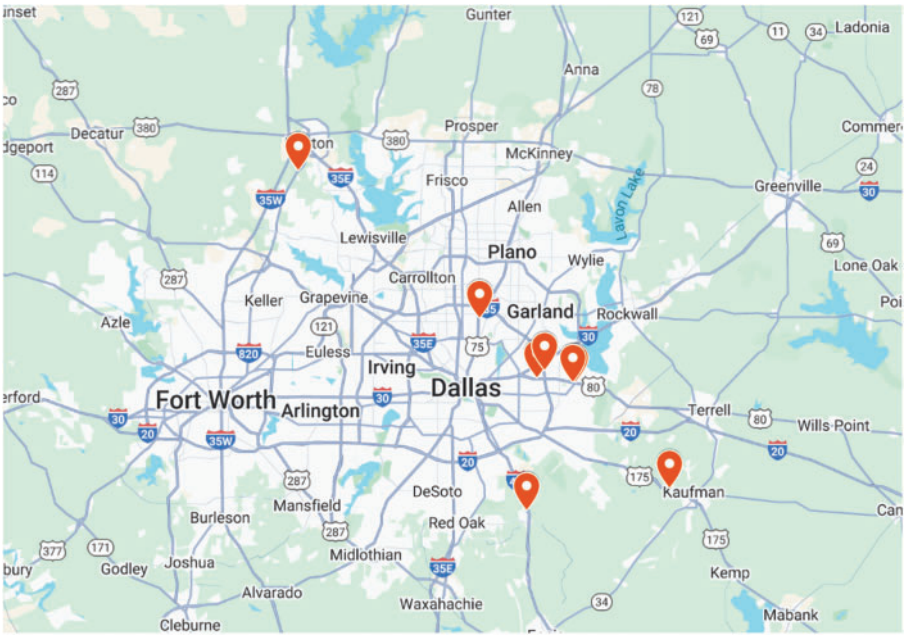

Figure 6. Bridge locations

Data Collection and Bridge Description

Field data was collected from eight different bridges in Texas using GPR and IE to assess the selected concrete bridge decks. Fig. 6 shows the locations of these bridges on Google Maps. Two common deck construction types encountered were cast-in-place (CIP) concrete over precast concrete panels (PCPs), often used in combination in composite systems where the CIP concrete is poured on top of the PCP. The characteristics, along with the NBI deck condition rating of each bridge, are summarized in Table 1.

Each bridge presented unique structural features and challenges, creating a diverse dataset for subsequent analysis and model development. To facilitate the NDE work, the Texas DOT personnel implemented traffic control measures. Longitudinal grid lines, spaced 760 mm apart, were marked on the bridge deck to guide NDE scanning. A truck-mounted GPR system, equipped with two 2.6 GHz antennas, was used to scan the bridge decks at a speed of 2.2 m/s, significantly reducing the time required compared to traditional methods. For IE scanning, 760 mm grid intervals were used with the test head pressed against the deck, providing additional subsurface condition data to complement the GPR findings. Fig. 7 shows the NDE data collection for bridge 6.

Clustering Workflow

The overall clustering workflow used in this study is summarized in Fig. 8. It begins with database preparation and data preprocessing, which includes exploratory data analysis (EDA), data cleaning, and normalization. EDA was performed to identify outliers and understand the distribution of features such as two-way travel time (TWTT), amplitude, and frequency. Normalization was applied to scale the features between 0 and 1.

Following preprocessing, cluster validation techniques were applied to determine the optimal number of clusters. The Elbow Method was used to identify the point of diminishing returns in within-cluster variance, providing a visual guide for selecting an efficient number of clusters. The Silhouette Score quantified how well-separated the clusters were, ensuring good cohesion and separation. The Bayesian information criterion (BIC) was used specifically for the GMM to strike a balance between model fit and complexity. For FCM clustering, the fuzzy partition coefficient (FPC) was employed to evaluate the clarity of the fuzzy cluster assignments. These methods were selected because they are widely accepted for evaluating the quality of clustering across both hard and soft clustering models.[29,34,35]

Table 1. Bridge description

Bridge name	Designation	Location	Year built	NBI deck condition rating	Deck type	Girder type	Deck area (m^2)
I-635 Bridge	Bridge 1	Mesquite, TX	2024	N/A	CIP	Composite steel deck	1,079
US 75 Pedestrian Underpass	Bridge 2	Dallas, TX	2023	N/A	CIP atop steel panel	None (cable-supported)	274
Westbound (WB) US 175 Big Brushy Creek	Bridge 3	Kaufman, TX	1950	5	CIP	Flat slab	2,044
WB US 80 at SH 352	Bridge 4	Sunnyvale, TX	2012	7	CIP atop PCP	Concrete I-girder	1,917
EB & WB US 80 Main Lanes at Stream 2B6	Bridge 5	Mesquite, TX	2012	4	CIP atop PCP	Concrete U–beams	985
US 377 over Hickory Creek Relief	Bridge 6	Denton, TX	1942	4	CIP	Steel I-girder	677
BI 45 at Ten Mile Creek Relief	Bridge 7	Dallas, TX	2024	N/A	CIP atop PCP	Concrete I-girder	722
Eastbound (EB)US 80 at SH 352	Bridge 8	Sunnyvale, TX	2012	6	CIP atop PCP	Concrete I-girder	1,917

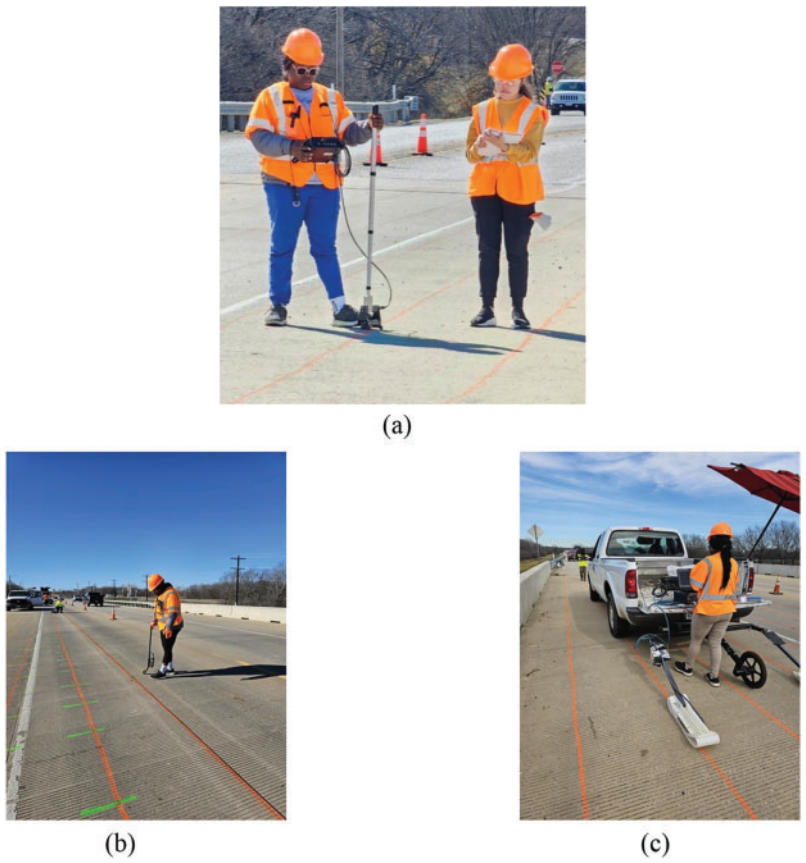

Figure 7. NDE scanning. (a) IE scanning, (b) GPR scanning gridlines, and (c) GPR deck scanning

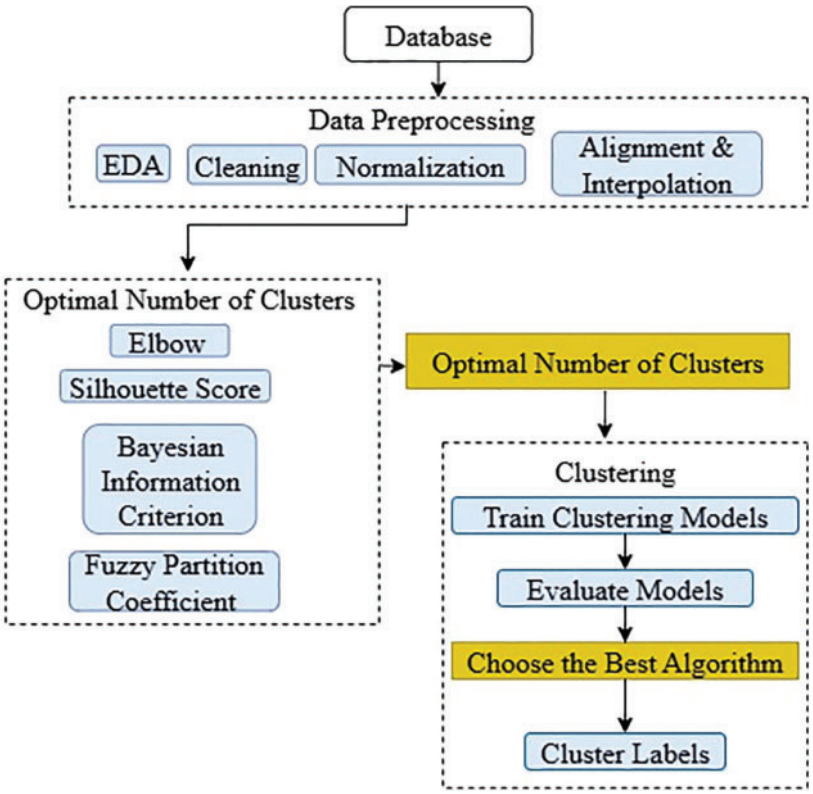

Figure 8. Clustering flowchart

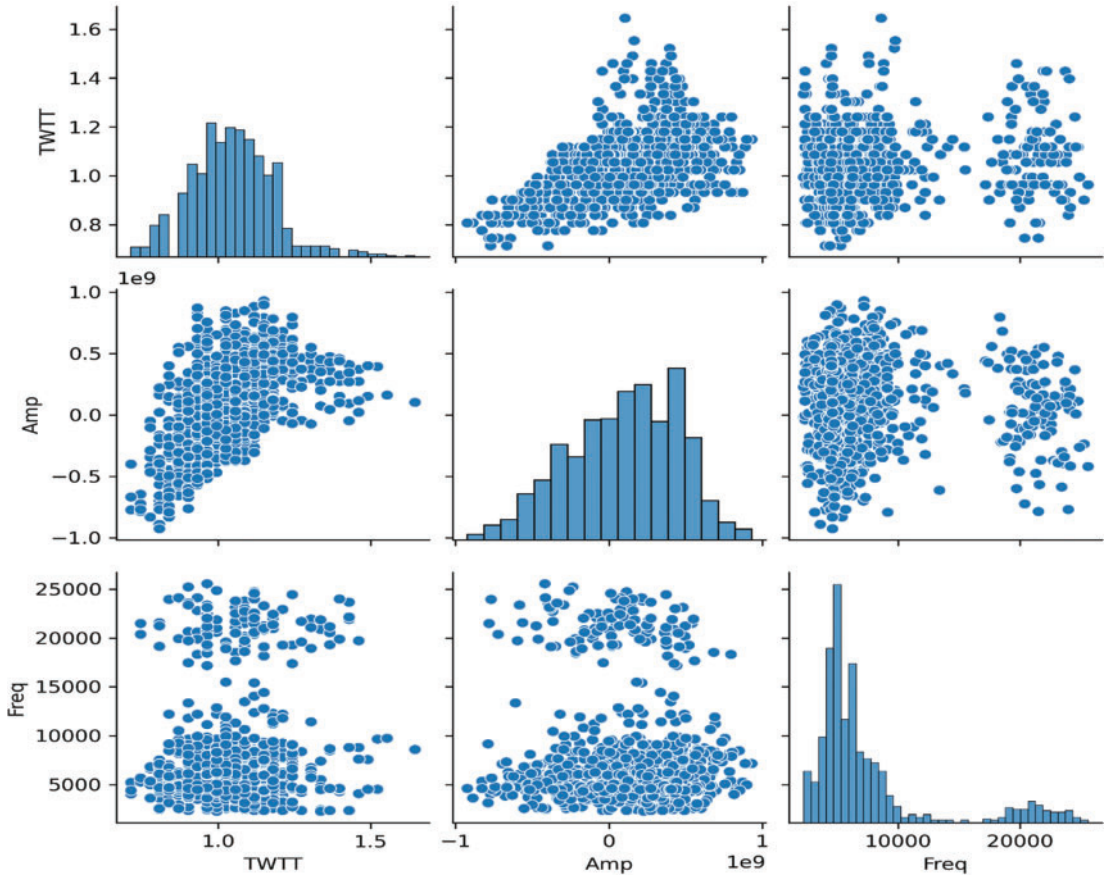

Figure 9. Raw GPR and IE feature distributions from test bridges before cleaning and normalization

Data Cleaning and Normalization

The collected GPR and IE data were preprocessed to ensure accuracy, consistency, and reliability. The first step involved data visualization to understand distribution patterns and detect anomalies. Noise and outliers were removed to enhance data quality. Feature normalization was applied, using Eq. (1), to ensure that TWTT, amplitude, and IE frequency values were within a standardized range of 0 to 1.[36] Histograms and scatter plots were generated to examine the raw feature distributions prior to normalization (Fig. 9). The result of the normalization process is shown in Fig. 10, illustrating consistent feature scaling suitable for subsequent analysis

$$X' = \frac{X - \min(X)}{\max(X) - min(X)} \frac{X - \min(X)}{\max(X) - min(X)} \quad (1)$$

where X is the original data and X' is the normalized data.

Data Alignment and Interpolation

To enable clustering of fused features from both sensors, the GPR and IE data were spatially aligned using a grid-based approach. GPR data points, which had higher spatial density, were retained as the reference grid. Each IE data point was matched to its nearest GPR neighbor based on spatial proximity using Euclidean distance.[37,38] In cases where multiple IE points mapped to the same GPR location, their values were averaged. For missing sensor values in sparse areas, inverse distance weighted interpolation was applied.[39,40] This allowed all features, including TWTT and amplitude from GPR and frequency from IE, to be combined for each grid cell. The resulting fused dataset maintained consistent x–y coordinates, ensuring reliable clustering across the combined feature space. This process ensured that all sensor readings were accurately mapped and spatially coherent, as demonstrated in the cluster distribution plots.

Cluster Number Determination

Since labeled condition states are not available for the GPR and IE data, supervised learning methods cannot be applied. Therefore, unsupervised learning techniques are necessary to discover inherent patterns and groupings in the dataset without predefined labels.[41,42] Selecting the optimal number of clusters (k) is a critical step in unsupervised learning, as it directly influences the quality and interpretability of the resulting clusters. The Elbow Method, Silhouette Score analysis, BIC, and FPC techniques were employed to determine the most suitable number of clusters for the integrated GPR and IE dataset.[35,34,28,29]

The Elbow Method involves plotting the within-cluster sum of squares for the selected features (TWTT, amplitude,

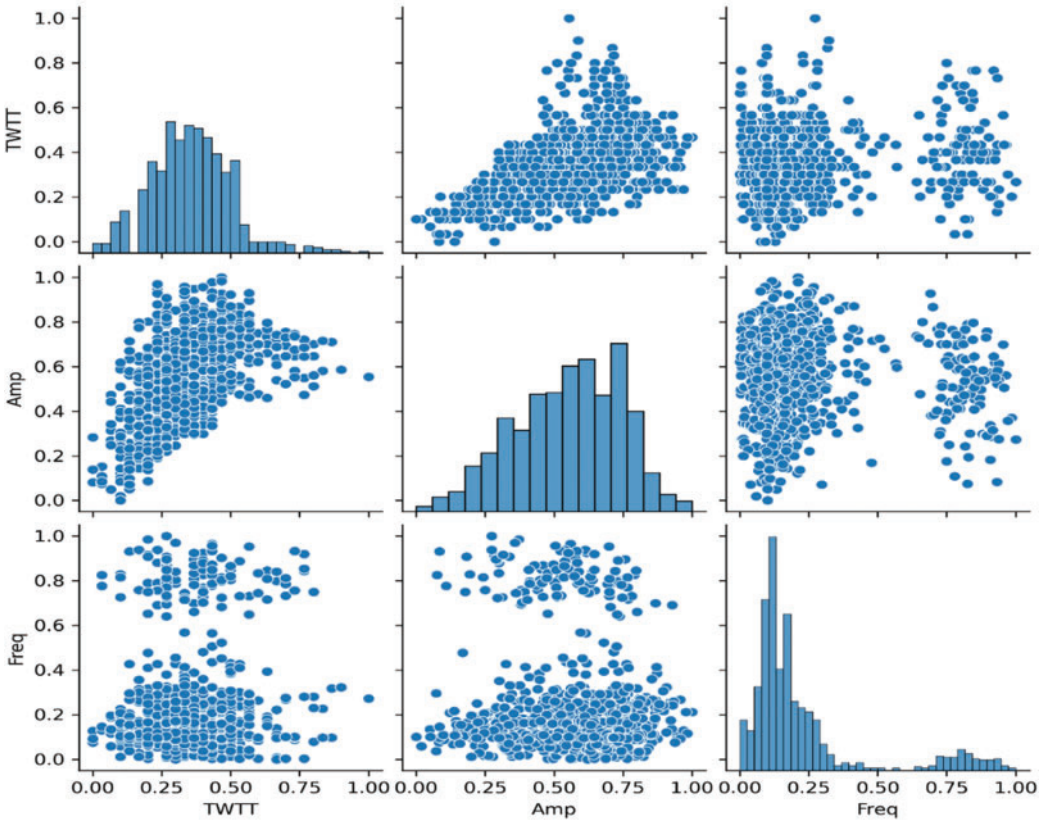

Figure 10. Normalized GPR and IE features from test bridges after preprocessing

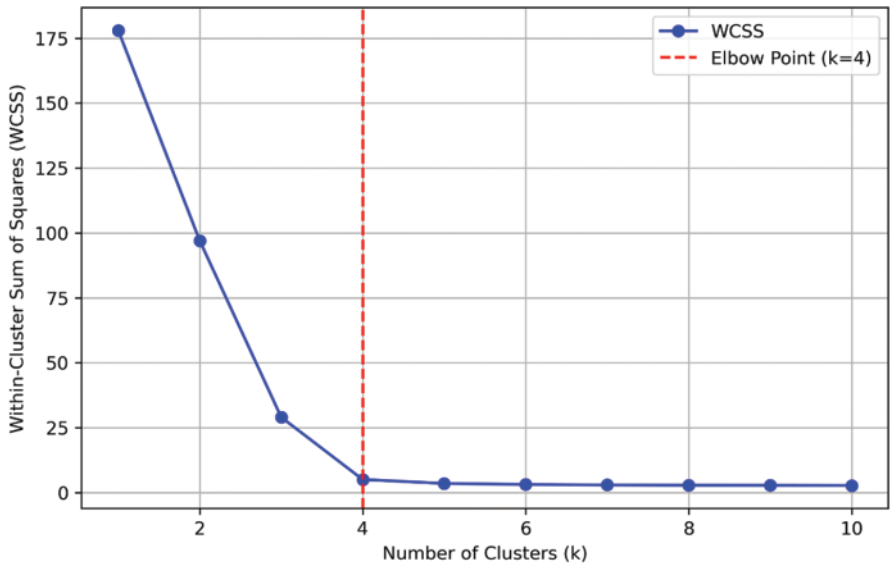

Figure 11. Elbow plot for K-means clustering

and IE frequency) against different values of "k." The point where the curve begins to flatten, referred to as the "elbow," indicates an optimal trade-off between compactness and model complexity. As shown in Fig. 11, the elbow occurs at k = 4, suggesting that four clusters provide an efficient representation of the dataset without overfitting. The Silhouette Score measures how well each data point fits within its assigned cluster relative to other clusters. A higher silhouette score indicates better cohesion within clusters and greater separation between clusters. As shown in Fig. 12, the average silhouette score reaches its maximum value at k = 4, further supporting this choice.

For the GMM, BIC was used to evaluate model fitness while removing excessive complexity. The lowest BIC value was observed at k = 4 (Fig. 13), indicating that this configuration achieved the best balance between data fit and parameter count. In the case of FCM, FPC was used to evaluate the clarity of the clustering structure. As expected,

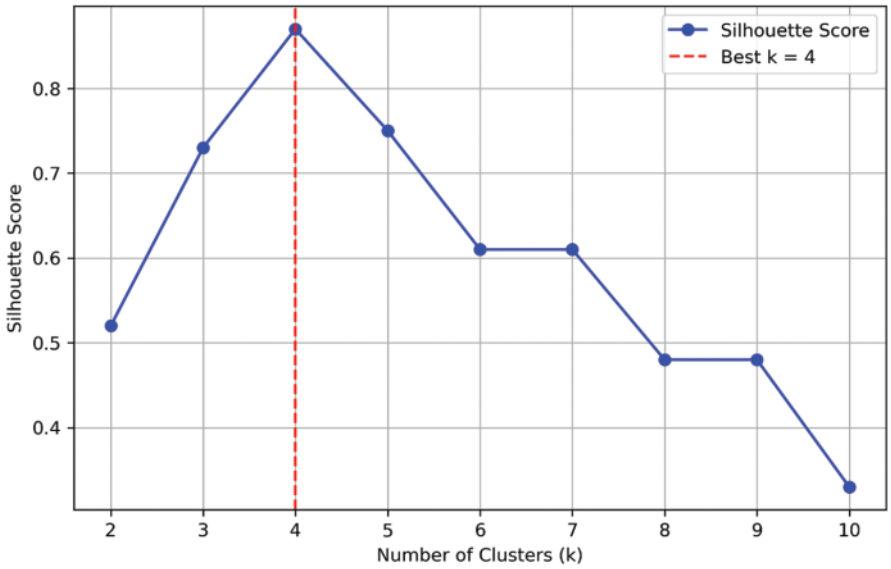

Figure 12. Silhoutte score versus number of clusters (K-means)

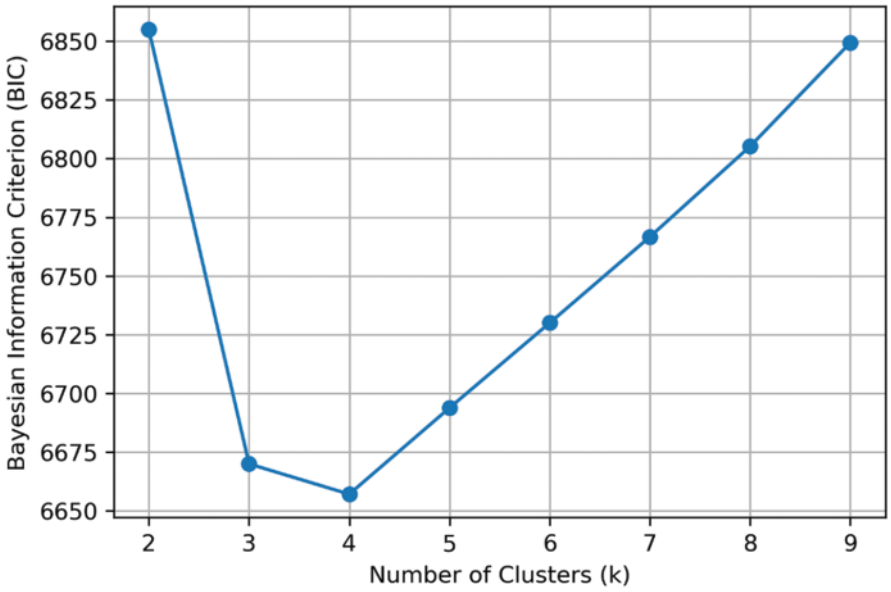

Figure 13. BIC versus number of clusters (GMM)

the FPC decreased as "k" increased, with the highest value observed at k = 2 (Fig. 14). However, the Elbow Method, Silhouette Score, and BIC consistently identified k = 4 as optimal. Thus, this value was used to configure the clustering algorithms in the subsequent analysis.

Clustering Model Development

After determining the optimal number of clusters (k = 4), four different clustering algorithms were used to identify patterns across the combined dataset from the eight bridges: K-Means, DBSCAN, GMM, and FCM. Each algorithm was selected for its unique strengths in identifying patterns and handling different data distributions. K-Means was chosen for its simplicity and efficiency in partitioning well-separated data.[28] DBSCAN was included due to its robustness in identifying clusters of arbitrary shape and handling noise points effectively.[29] The GMM algorithm was employed for its probabilistic clustering capabilities, which allow soft assignment of points to multiple clusters.[30] Finally, FCM was used to model the uncertainty and overlapping nature of bridge condition states, making it suitable for condition assessment applications involving gradual transitions between states.[42,41] The models were developed using Python (version 3.12.2, 2024) with supporting libraries, including Scikit-Learn for clustering, NumPy and Pandas for data manipulation, and Matplotlib for visualization. Parameter tuning was applied for each algorithm to optimize performance and ensure accurate cluster formation.

Collectively, the four clustering algorithms were applied systematically to the eight-bridge dataset to capture different

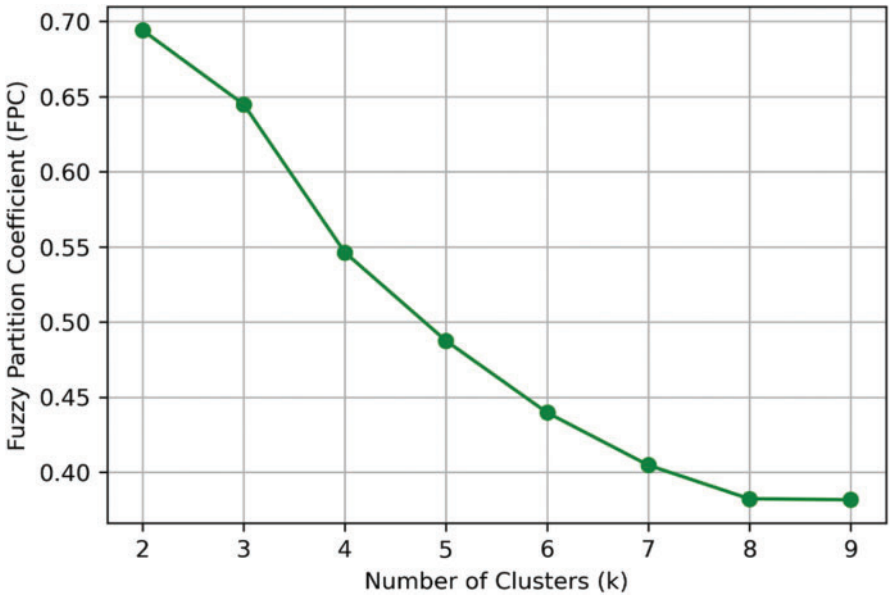

Figure 14. FPC versus number of clusters (FCM)

aspects of the defect patterns, ranging from sharp partitions to ambiguous transitions, providing complementary insights for subsequent analysis. Although the clustering models were trained on the combined data, the resulting cluster labels were also linked to individual bridge decks to show how these patterns manifest on specific bridges. The rationale and mechanics of each clustering method are summarized below.

K-means clustering

The primary objective of K-Means is to minimize WCSS from Eq. (2), which quantifies the total squared distance between each data point and its respective centroid.[28]

$$WCSS = \sum_{i=1}^{K} \sum_{x_j \in C_i} ||x_j - \mu_i||^2 \tag{2}$$

where $C_i =$ is the ith cluster, $\mu_i =$ centroid of cluster I, x_j is the data points in cluster i.

The K-Means algorithm operates in two main steps: (1) assigning each point to the nearest centroid using Euclidean distance; and (2) updating each centroid to the mean of its assigned points. These steps are repeated iteratively until the centroids stabilize and the model converges. On the combined dataset, K-Means separated the data into four clusters, differentiating patterns associated with intact concrete, suspected delamination, and transitional conditions. The algorithm was applied to the whole dataset, and the resulting labels were linked back to individual bridges.

DBSCAN

DBSCAN identifies clusters based on the local density and uses two key parameters: (1) epsilon, ε, which defines the radius of the neighborhood around each point; and (2) minPts, the minimum number of points required to form a dense region. A point is considered a core point if it has at least minPts points within its ε-neighborhood. Points not reachable from any core point are labeled as noise or outliers. DBSCAN is particularly effective for detecting clusters of arbitrary shapes and for handling datasets with noise or spatial variability, such as those found in GPR and IE scanning. However, its performance is highly dependent on selecting appropriate values for ε and minPts.

In this study, DBSCAN was applied to the combined GPR and IE dataset (TWTT, amplitude, and IE frequency) from the eight bridges to identify dense regions in feature space and detect potential outliers. The ε and minPts were tuned through trial and error, guided by the observed density distribution in the dataset. The goal was to isolate densely packed regions corresponding to potential defect zones while minimizing the impact of sparsely distributed noise points. The neighborhood function used by DBSCAN is defined in Eq. (3):[29]

$$\begin{aligned} \text{Neighbor}\,(x_i, \varepsilon) &= \left\{x_j || x_i - x_j| \le \varepsilon\right\} \left(x_i, \varepsilon\right) \\ &= \left\{x_j || x_i - x_j| \le \varepsilon \right. \end{aligned} \tag{3}$$

where x_i and $x_j =$ are the data points, $\|x_i - x_i\|$ is the Euclidean distance between them, and a a point x_i is a core point if |Neighbor (x_i, ε) | ≥ minPts.

GMM

GMM assumes that the dataset is generated from a mixture of multiple Gaussian distributions, where each distribution represents a potential cluster. Unlike K-Means, which exclusively allocates each data point to one cluster, GMM adopts a probabilistic approach, assigning each point a degree of membership across all clusters. This flexibility makes GMM especially effective in situations where cluster boundaries are not well separated. GMM uses the Expectation-Maximization (EM) algorithm, which iteratively refines the model parameters—mean vectors (μ_k),

covariance matrices (Σ_k), and mixture weights (k)—to maximize the likelihood of the observed data. During the Expectation step, the model estimates the responsibility that each Gaussian component takes for each data point. In the Maximization step, these responsibilities are used to update the model parameters until convergence.

In this study, GMM was applied to the combined GPR and IE dataset from the eight bridges. The number of Gaussian components (k = 4) was determined based on the BIC, which balances model fit with complexity. The log-likelihood function maximized by the EM algorithm is given by Eq. (4):[30]

$$\mathcal{L}(\theta) = \prod_{i=1}^{N} \sum_{k=1}^{K} \pi_k N(x_i|\mu_k, \Sigma_k) \tag{4}$$

where $\mathcal{L}(\theta)$ is the likelihood of the observed data, π_k is the weight of the kth Gaussian component, $N(x_i|\mu_k, \Sigma_k)$ is the Gaussian probability density function, with mean μ_k and covariance Σ_k, $x_i =$ is the ith data point, and μ_k and Σ_k the parameters of the kth Gaussian.

FCMs

FCM is a variation of K-Means clustering that allows each data point to belong to multiple clusters with varying degrees of membership. Instead of assigning a point to a single cluster, FCM calculates a membership grade that indicates the degree of association between each data point and every cluster. The objective of FCM is to minimize the weighted sum of distances between each point and the cluster centroids, with each point's contribution to the objective function being weighted by its membership grade. The objective function for FCM is given in Eq. (5)[43]

$$J_m = \sum_{i=1}^{N} \sum_{j=1}^{C} u_{ij}^m ||x_i - C_j||^2 \tag{5}$$

where N is the number of data points, C the number of clusters, u_{ij} the membership grade of data point x_i in cluster c_j, and m is the fuzziness parameter (usually set to 2).

In this study, FCM was applied to the combined GPR and IE dataset (TWTT, amplitude, IE frequency) of the eight bridges. The fuzziness parameter m was set to 2, and the number of clusters was fixed at k = 4 based on prior evaluation criteria.

Results and Discussion

Clustering performance evaluation

The quality of the clustering results was first assessed to ensure they are technically sound and meaningful. Table 2 summarizes the Silhouette Scores and Davies–Bouldin Indices for each algorithm. The former measures how well points fit within their assigned cluster compared to others; higher scores indicate better-defined clusters. The latter measures the average similarity between each cluster and its most similar cluster, with lower values indicating better separation.

Among the algorithms, DBSCAN resulted in the highest Silhouette Score (0.98), reflecting its ability to form tight and dense clusters. However, since it focuses only on dense regions and labels many points as noise, it was less suitable for mapping global bridge deck conditions. Approximately 18% of the data points were considered as noise and excluded from the Silhouette Score calculation, contributing to the high value reported. Due to this limitation, DBSCAN was not used to generate the condition maps.

To ensure complete spatial coverage, K-Means clustering was selected for visualization purposes, as it assigns all data points to clusters and ensures full spatial coverage of the bridge decks. This makes K-Means more appropriate for interpreting overall condition trends across the bridge decks. FCM achieved the lowest Davies–Bouldin Index (0.82), indicating good separation between clusters and smooth transitions across boundaries. Together, these performance metrics validate the robustness of the clustering approaches and justify their application in subsequent condition analysis. The clustering results from DBSCAN, GMM, and FCM were used to validate the consistency of severity zone identification across methods. Despite algorithmic differences, key patterns were consistently observed. Cluster 1 corresponded to areas of severe deterioration, and Cluster 4 indicated sound concrete. This cross-method agreement reinforces the robustness of the K-Means-based condition maps used in the final analysis.

Cluster labeling and interpretation

After confirming their performance, the clusters were analyzed and interpreted to relate them to the physical conditions of the bridge decks. Each cluster generated by the different algorithms was examined in the context of its defining features, and the following interpretations were derived:

1. Cluster 1 (mixed amplitude and TWTT, high-frequency variability): This cluster exhibited signal variability in both GPR and IE data, reflecting heterogeneous rebar condition. Such variability is often associated with localized corrosion, differences in moisture content, or partial delamination. These patterns align with findings on bridge decks affected by progressive deterioration and corrosion.[1,44,45,21]
2. Cluster 2 (low amplitude, high TWTT, low frequency): The low amplitude and high TWTT indicate areas of the bridge decks where there might be voids or delaminations, and rebars are located at greater depths. These regions were marked as potential delamination zones.[46] Though standard IE theory predicts that shallower delamination should yield higher resonant frequencies, several field and lab studies reported that shallow delamination in in-service concrete decks often corresponds to lower IE frequencies.[47,48,26] This is likely due to energy loss, poor bonding at the delaminated interface, and wave scattering, which affect the dominant frequency response.

Table 2. Clustering evaluation metrics and scores

Metrices	K-Means	DBSCAN	GMM	FCM
Silhouette Score	0.72	0.98	0.93	0.96
Davies–Bouldin Index	0.85	0.97	0.95	0.82

Table 3. Summary of cluster labels

Cluster no.	Condition
1	Corrosion-prone/deteriorating areas
2	Potential delamination
3	Sound but shallow rebar
4	Well-bonded concrete

3. Cluster 3 (high amplitude, very low TWTT, high frequency): The high GPR amplitude and very low TWTT point to minimal signal attenuation and minimal concrete cover. Concurrently, high IE frequency responses are indicative of well-bonded, defect-free concrete. These zones may contain shallow rebars that could become exposed in the future, warranting periodic monitoring to ensure long-term durability.[49,24]
4. Cluster 4 (high amplitude, low TWTT, high frequency): High amplitude and low TWTT GPR data indicate dense and well-bonded concrete, characterizing regions with minimal subsurface defects or good quality concrete.[46,50] The corresponding high IE frequency further confirms the material integrity.

These interpretations link the cluster outputs to potential defect zones, rebar issues, or other conditions that may compromise the integrity of the bridges. These findings are summarized in Table 3, which groups the clusters based on their associated conditions.

By mapping the clustering results back to each bridge deck, distinct defect patterns were identified and compared across structures. Fig. 15 presents the proportion of each cluster across the eight bridges, clearly showing how different bridges exhibit distinct dominant condition patterns. For example, Bridge 1 primarily consisted of Cluster 4 (well-bonded concrete), suggesting generally good concrete quality, with scattered areas of Cluster 3 (sound but shallow rebar) and Cluster 1 (corrosion-prone), indicating localized shallow rebar and potential corrosion zones (Fig. 16). Bridge 2 exhibited a predominance of Cluster 3, highlighting areas in good condition but with a reduced rebar cover that warrant periodic monitoring (Fig. 17). In contrast, Bridge 3 was dominated by Cluster 1 (corrosion-prone), followed by noticeable occurrences of Cluster 2 (potential delamination) and a few areas of Cluster 3, indicating widespread deterioration across the deck (Fig. 18). Some clusters were absent or minimal on certain bridges, showing the ability of the clustering to reveal bridge-specific condition patterns. Such findings support the prioritization of inspections and maintenance, as inspectors can focus on bridges with higher proportions of damage-prone clusters, rather than treating all bridges equally.

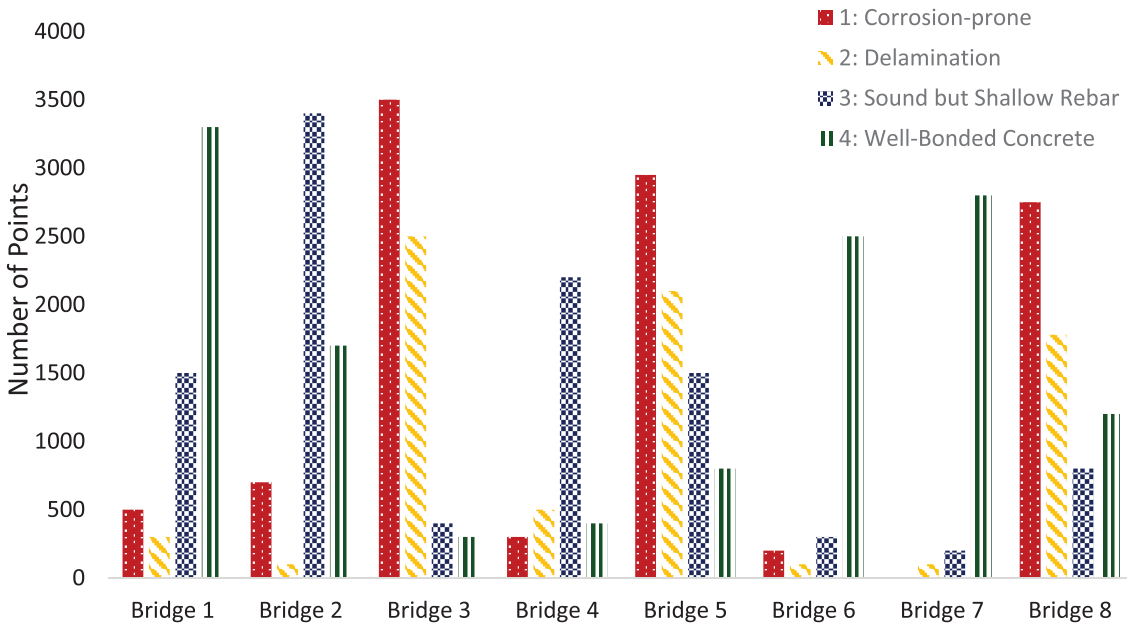

Figure 15. Distribution of clusters across bridges

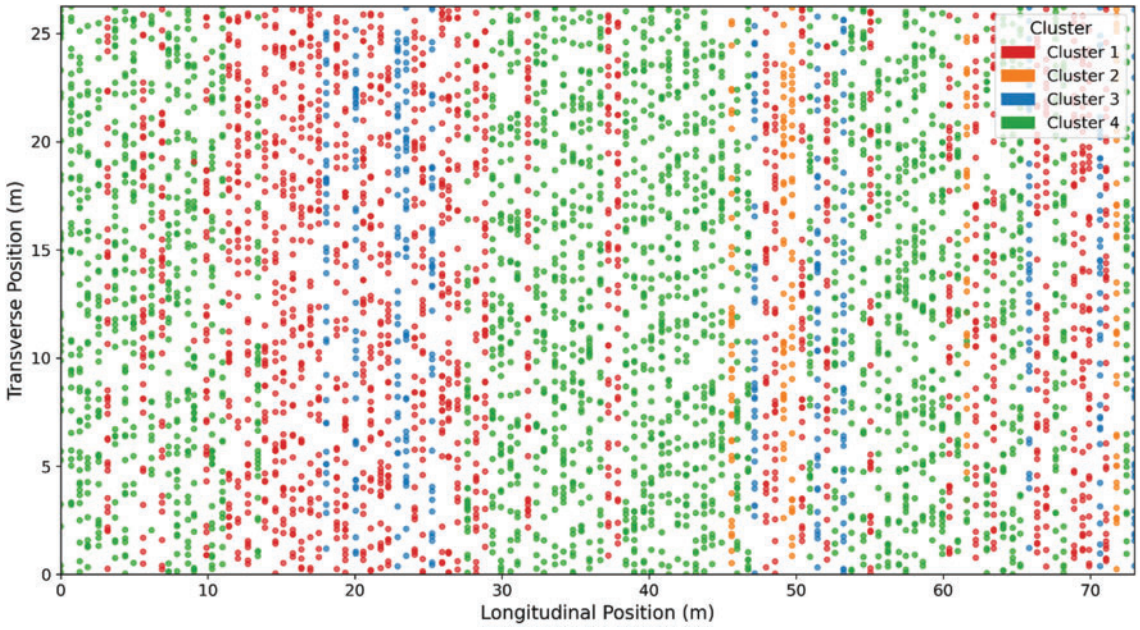

Figure 16. Spatial distribution of clusters for bridge 1

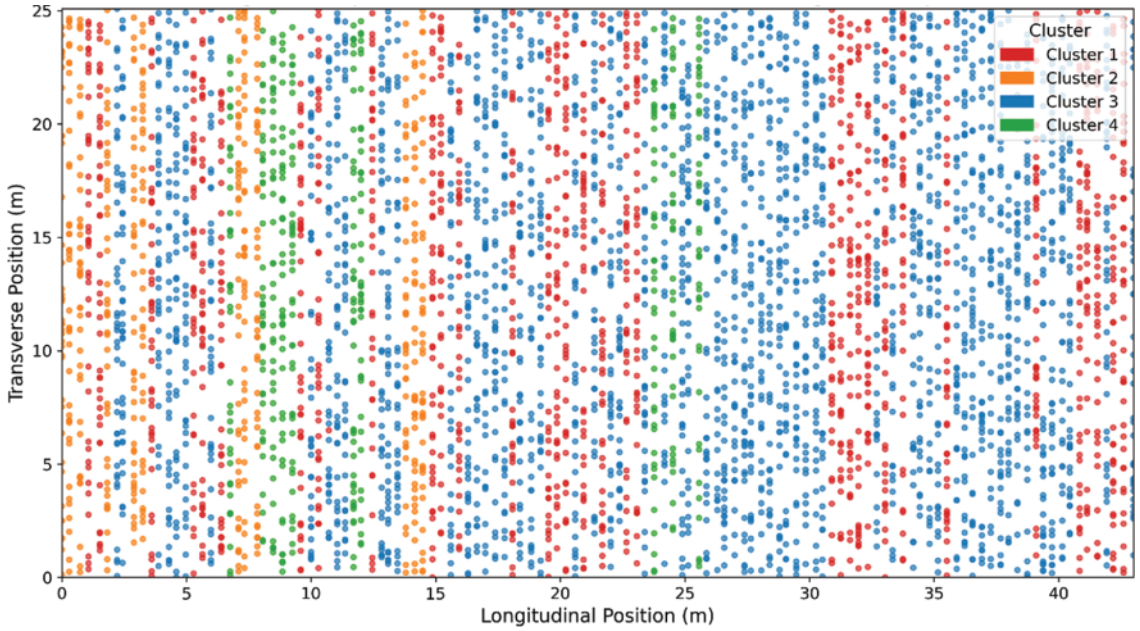

Figure 17. Spatial distribution of clusters for bridge 2

Figs. 16–18 illustrate the spatial distribution of clusters across the deck surfaces of Bridges 1, 2, and 3. These maps help engineers identify localized damage zones. Thus, instead of adopting similar maintenance strategies across the entire bridge deck, more attention may be given to areas most likely to exhibit damage and plan targeted maintenance, thereby improving efficiency and reducing costs.

The clustering approach offers a highly comprehensive and objective interpretation of bridge conditions, surpassing the limitations of traditional contour maps, which often focus on single features. By integrating multiple features and automatically classifying severity levels, clustering enables: (1) enhanced understanding of subsurface conditions; (2) Reduced reliance on subjective visual inspections; (3) targeted field investigations and cost-efficient maintenance; (4) integration into bridge management systems or GIS-based platforms; and (5) foundation for developing consistent condition ratings (e.g., fuzzy logic models). While the clustering framework successfully identified consistent deterioration patterns across eight bridges, most of these structures were relatively new (constructed within the past 10 to 15 years), with only two representing older bridge decks. As such, the generalizability of the four derived clusters to significantly older infrastructure remains uncertain. Bridge decks with long-term deterioration histories may exhibit different signal characteristics and degradation patterns. Therefore, direct

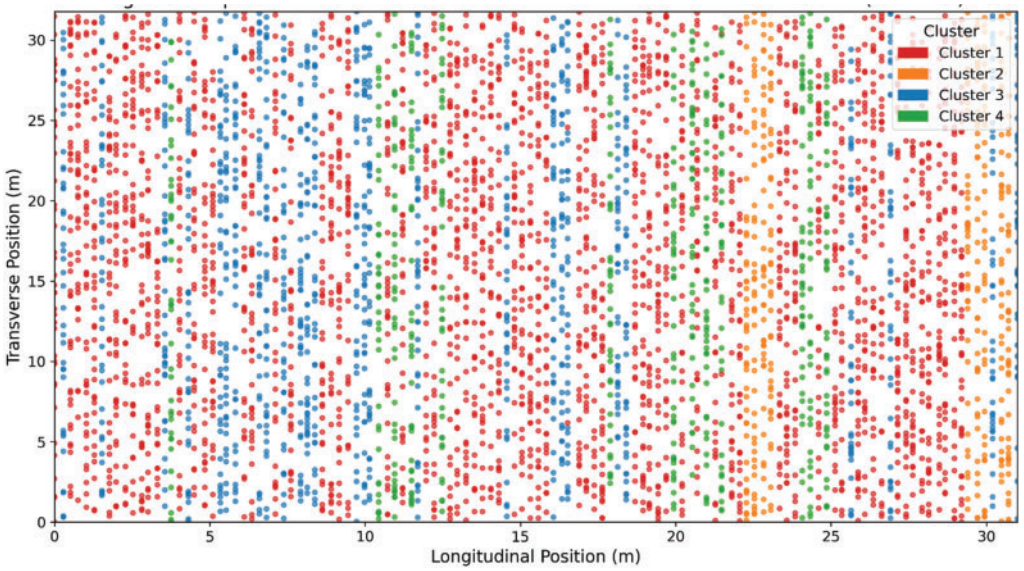

Figure 18. Spatial distribution of clusters for bridge 3

application of these cluster interpretations to older bridges without further validation should be carefully considered.

Conclusions

The following conclusions may be made based on the findings from this study:

1. The clustering-based framework successfully processed and fused GPR and IE data from eight bridges, enabling the automated identification of subsurface condition patterns.
2. By applying four unsupervised clustering algorithms (K-Means, DBSCAN, GMMs, and FCMs), the study successfully identified meaningful subsurface defect patterns.
3. The DBSCAN framework resulted in the highest Silhouette Score (0.98), while FCM recorded the lowest Davies–Bouldin Index (0.82), demonstrating the effectiveness of clustering techniques in identifying distinct defect zones.
4. Four consistent clusters were identified: Cluster 1 (corrosion-prone), Cluster 2 (delamination), Cluster 3 (shallow rebar), and Cluster 4 (well-bonded concrete), with repeatable interpretation across algorithms.
5. Cluster mapping enabled clear visualization of damage zones and supported targeted maintenance planning, surpassing traditional evaluation methods.
6. The spatial distribution of clusters reflected real-world deterioration trends: older bridges exhibited more severe defects, while newer bridges showed predominantly intact concrete.
7. Clustering enhances bridge condition assessments by supplementing visual inspections with objective subsurface data, improving reliability and reducing subjectivity.
8. The framework supports standardization in bridge deck evaluation, offering a scalable tool for DOTs to implement data-driven, transparent decision-making processes.

Recommendations for follow-up work

1. Incorporate the clustered condition labels into fuzzy inference systems or bridge condition rating models to support objective scoring.
2. Expand the dataset by applying the framework to a broader range of bridge types and geographical regions to assess its generalizability.
3. Integrate additional NDE techniques such as half-cell potential or ultrasonic pulse velocity to improve the classification of overlapping or uncertain defects.
4. Embed the clustering framework into GIS platforms to support real-time visualization, condition monitoring, and proactive maintenance scheduling.
5. Conduct periodic scans of bridges over time to explore how clustered patterns evolve, enabling predictive deterioration modeling and lifecycle management.
6. External validation through coring was not feasible for this study due to restrictions on destructive testing of in-service bridges. Instead, the cluster interpretations were guided by known signal behaviors in TWTT, amplitude, and IE frequency, and were consistent with deterioration mechanisms reported in prior studies.[1,46,45] The observed alignment between clustering results and expected field conditions, such as more severe clusters on older decks, supports the reliability of the findings. Future research should incorporate selective destructive or semi-destructive testing to directly confirm subsurface defect states and further validate the clustering predictions.
7. Future research should apply the clustering framework to older bridge decks with more advanced deterioration to evaluate whether the identified cluster patterns

remain consistent across different bridge ages and condition states.

Data availability statement

The data presented in this study are available on request from the corresponding author.

References

[1] Gucunski N, Imani A, Romero F, et al. *Nondestructive Testing to Identify Concrete Bridge Deck Deterioration (SHRP 2 Report S2-R06A-RR-1)*. Transportation Research Board; 2013. doi:10.17226/22771.

[2] American Society of Civil Engineers. *2021 Report Card for America's America's Infrastructure: A Comprehensive Assessment of America's America's Infrastructure (Executive Summary)*. Reston, VA: American Society of Civil Engineers; 2021. https://infrastructurereportcard.org.

[3] Federal Highway Administration (FHWA). *Recording and Coding Guide for the Structure Inventory and Appraisal of the Nation's Bridges* (Report No. FHWA-PD-96-001). U.S. Department of Transportation; 2021. Retrieved from: https://www.fhwa.dot.gov/bridge/mtguide.pdf.

[4] Washer GA, Fuchs PA. Developments in the use of infrared thermography for the condition assessment of concrete. *Proceedings of the International Symposium on Non-Destructive Testing in Civil Engineering (NDT-CE)*; 2015; Berlin, Germany.

[5] Dinh K, Zayed T. GPR-based fuzzy model for bridge deck corrosiveness index. *J Perform Const Facil*. 2015; 29(4):04014101. doi:10.1061/(ASCE)CF.1943-5509.0000815.

[6] Federal Highway Administration. *Improving Bridge Performance with Nondestructive Evaluation Technologies (Report No. FHWA-HRT-25-009)*. McLean, VA: U.S. Department of Transportation, Federal Highway Administration, Turner-Fairbank Highway Research Center; 2024. https://highways.dot.gov/sites/fhwa.dot.gov/files/FHWA-HRT-25-009.pdf.

[7] Omar T, Nehdi ML. Condition assessment of reinforced concrete bridges: current practice and research challenges. *Infrastructures*. 2018;3(3):36. doi:10.3390/infrastructures 3030036.

[8] Gucunski N, Pailes BM, Kim J, Azari H, Dinh K. Capture and quantification of deterioration progression in concrete bridge decks through periodical NDE surveys. *J Infrastruct Syst*. 2017;23(1):04016029. doi:10.1061/(ASCE) IS.1943-555X.0000321.

[9] Gucunski N, Romero F, Kruschwitz S, Feldmann R, Parvardeh H. *Comprehensive Bridge Deck Deterioration Mapping of Nine Bridges by Nondestructive Evaluation Technologies (Final Report)*. Rutgers, The State University of New Jersey, Center for Advanced Infrastructure and Transportation; 2011.

[10] Gucunski N, Romero F, Kruschwitz S, Feldmann R, Abu-Hawash A, Dunn M. Multiple complementary nondestructive evaluation technologies for condition assessment of concrete bridge decks. *Transport Res Rec: J Transport Res Board*. 2010;2201(1):34–44. doi:10.3141/2201-05.

[11] Hugenschmidt J, Mastrangelo R. GPR inspection of concrete bridges. *Cem Concr Compos*. 2006;28(4):384–392. doi:10.1016/j.cemconcomp.2006.02.016.

[12] Brown MC, ElBatanouny M, Bektaş B, Azari H, Foden AJ, Imani A, et al. *Incorporating Nondestructive Evaluation Methods into Bridge Deck Preservation Strategies (FHWA Publication No. FHWA-HRT-24-186)*. McLean, VA: U.S. Department of Transportation, Federal Highway Administration, Turner-Fairbank Highway Research Center; 2024. doi:10.21949/1521524.

[13] Scherr J, Grosse C. Delamination detection on a concrete bridge deck using impact echo scanning. *Struct Concr*. 2021;22(2):806–812. doi:10.1002/suco.202000415.

[14] American Society for Testing and Materials (ASTM). *ASTM D6432-19: Standard Guide for Using the Surface Ground Penetrating Radar Method for Subsurface Investigation*. West Conshohocken, PA: ASTM International; 2019. doi:10.1520/D6432-19.

[15] Geophysical Survey Systems, Inc. (GSSI). *Concrete HandBook: GPR Inspection of Concrete (MN72-367 Rev. H)*. Nashua, NH: Geophysical Survey Systems, Inc.; 2017.

[16] Hasan MI, Yazdani N. Ground penetrating radar utilization in exploring inadequate concrete covers in a new bridge deck. *Case Stud Construct Mat*. 2014;1:104–114. doi:10.1016/j.cscm.2014.04.003.

[17] Hugenschmidt J. Concrete bridge inspection with a mobile GPR system. *Construct Build Mat*. 2002;16(3):147–154. doi:10.1016/S0950-0618(02)00003-4.

[18] Gagarin N, Goulias D, Mekemson J. Condition rating of bridge decks with fuzzy sets modeling for SF-GPR surveys. *Remote Sens*. 2023;15(14):3631. doi:10.3390/rs15143631.

[19] Ibrahim A, Abdelkhalek S, Zayed T, Qureshi AH, Abdelkader EM. A comprehensive review of the key deterioration factors of concrete bridge decks. *Buildings*. 2024;14(11):3425. doi:10.3390/buildings14113425.

[20] La HM, Gucunski N, Kee SH, Nguyen LV. Data analysis and visualization for the bridge deck inspection and evaluation robotic system. *Visualizat Eng*. 2015;3(1):6. doi:10.1186/s40327-015-0017-3.

[21] Mohamadi S, Lattanzi D, Azari H. Fusion and visualization of bridge deck nondestructive evaluation data via machine learning. *Front Mat*. 2020;7:576918. doi:10.3389/fmats.2020.576918.

[22] Python Software Foundation. *Python Language Reference, version 3.12.2*; 2024. https://www.python.org.

[23] Yoon Y-G, Kim C-M, Oh T-K. A study on the applicability of the impact-echo test using semi-supervised learning based on dynamic preconditions. *Sensors*. 2022;22:5484. doi:10.3390/s22155484.

[24] Zhang Y, Yin E, Li F, et al. Hierarchical feature fusion framework for frequency recognition in SSVEP-based BCIs. *Neur Netw*. 2019;119:1–9.

[25] Hoxha E, Feng J, Sanakov D, Gjinofci A, & Xiao J. Robotic inspection and characterization of subsurface defects on concrete structures using impact sounding. arXiv preprint arXiv:2208.06305; 2022.

[26] Jafari F, Dorafshan S. Comparison between supervised and unsupervised learning for autonomous delamination detection using impact echo. *Remote Sensing*. 2022;14(24):6307. doi:10.3390/rs14246307.

[27] Völker C, Shokouhi P. Clustering based multi sensor data fusion for honeycomb detection in concrete. *J Nondestruct Evaluat*. 2015;34(4):32. doi:10.1007/s10921-015-0307-7.

[28] Jain AK. Data clustering: 50 years beyond K-means. *Pattern Recognit Lett*. 2010;31(8):651–666. doi:10.1016/j.patrec.2009.09.011.

[29] Schubert E, Sander J, Ester M, Kriegel HP, Xu X. DBSCAN revisited, revisited: Why and how you should (still) use DBSCAN. *ACM Transact Database Syst*. 2017;42(3):1–21. doi:10.1145/3068335.

[30] Reynolds DA. Gaussian mixture models. In: Li SZ. (Ed.), *Encyclopedia of Biometrics*. Springer; 2015:827–832. doi: 10.1007/978-1-4899-7488-4_196.

[31] Fang F, Ouyang L, Meng Y, Xu Q, Chen J, Qiu L. Structural adaptive damage detection under uncertainty based on probability dissimilarity and moving average control chart. *Measurement*. 2024;225(1):114023. doi:10.1016/j.measurement.2023.114023.

[32] Pedram M, Taylor S, Hamill G, Robinson D. Quantification of subsurface defects in reinforced concrete of bridges by unsupervised segmentation of IR images. In: *Proceedings of the IABSE Symposium Istanbul 2023: Long Span Bridges*. Istanbul, Turkey: International Association for Bridge and Structural Engineering (IABSE); 2023:835–845. doi: 10.2749/istanbul.2023.0835.

[33] Omar T, Nehdi ML. Remote sensing of concrete bridge decks using unmanned aerial vehicle infrared thermography. *Automat Construct*. 2017;83(11):360–371. doi:10.1016/j.autcon.2017.06.024.

[34] Liu H, Zhang Y. Bridge condition rating data modeling using deep learning algorithm. *Struct Infrastruct Eng*. 2020;16(2):1–14. doi:10.1080/15732479.2020.1712610.

[35] Solla M, Fernández N, Elseicy A, Pais J. Clustering approach for crack detection in GPR data: influence of infilling material on detectability. *Case Stud Construct Mat*. 2025;22(10):e04782. doi:10.1016/j.cscm.2025.e04782.

[36] Han J, Kamber M, Pei J. *Data Mining: Concepts and Techniques*. 3rd ed. Burlington, MA: Morgan Kaufmann; 2011. doi:10.1016/C2009-0-61819-5.

[37] Zhou F, Chen Z, Liu H, Cui J, Spencer BF, & Fang G. Simultaneous estimation of rebar diameter and cover thickness by a GPR-EMI dual sensor. *Sensors*. 2018;18(9):2969. doi:10.3390/s18092969.

[38] Cotič P, Niederleithinger E, Stoppel M. *Unsupervised Fusion of Scattered Data Collected by a Multi-Sensor Robot on Concrete*. BAM, Berlin: GZfP-Jahrestagung 2014–Di.2.C.1; 2014.

[39] Pashoutani S, Zhu J, Sim C, Ramseyer C. Multi-sensor data collection and fusion using autoencoders in condition evaluation of concrete bridge decks. *J Infrastruct Preservat Resil*. 2021;2(1):18. doi:10.1186/s43065-021-00032-3.

[40] Lu GY, Wong DW. An adaptive inverse-distance weighting spatial interpolation technique. *Comput Geosci*. 2008;34(9):1044–1055. doi:10.1016/j.cageo.2007.07.010.

[41] Jiao Y, Liu H, Zhang P, Wang X, & Wei H. Unsupervised performance evaluation strategy for bridge superstructure based on fuzzy clustering and field data. *J Perform Constr*. 2020. doi:10.1061/(ASCE)CF.1943-5509.0001455.

[42] Sasmal S, Ramanjaneyulu K, & Gopalakrishnan S. Fuzzy logic-based condition rating of existing reinforced concrete bridges. *J Perform Constr Facil*. 2006;20(3):261–273. doi:10.1061/(ASCE)0887-3828(2006)20:3(261).

[43] Chang S-C, Chuang W-C, Jeng J-T. New interval improved fuzzy partitions fuzzy C-means clustering algorithms under different distance measures for symbolic interval data analysis. *Appl Sci*. 2023;13(22):12531. doi:10.3390/app132212531.

[44] Marzorati S, Todaro R, Cocco G, & Guadagnini M. Fusion and visualization of bridge deck nondestructive evaluation data for corrosion assessment. *Materials*. 2020;13(24):5769. doi:10.3390/ma13245769.

[45] Faris N, Zayed T, Abdelkader EM, Fares A. Corrosion assessment using ground penetrating radar in reinforced concrete structures: influential factors and analysis methods. *Automat Construct*. 2023;158:105130. doi:10.1016/j.autcon.2023.105130.

[46] Dinh K, Gucunski N, Kim J, Duong TH. Understanding depth–amplitude effects in assessment of GPR data from concrete bridge decks. *NDT & E Int*. 2016;83(2):48–58. doi:10.1016/j.ndteint.2016.06.004.

[47] Gucunski N, Imani A, Romero F, Kruschwitz S. Automated impact echo testing of concrete bridge decks: towards faster and more objective evaluations. In: *Transportation Research Board 94th Annual Meeting Compendium of Papers*. Washington, DC: Transportation Research Board; 2015.

[48] Momo MM. *Quantifying Shallow Depth Concrete Delaminations Using Impact Echo*. Master's thesis. The University of Texas at Arlington; 2020. https://rc.library.uta.edu/uta-ir/handle/10106/29606.

[49] Pashoutani S, Zhu J. Real depth-correction in ground penetrating radar data analysis for bridge deck evaluation. *Sensors*. 2023;23(2):1027. doi:10.3390/s23021027.

[50] Sengupta A, Guler SI, Shokouhi P. Interpreting impact echo data to predict condition rating of concrete bridge decks: a machine-learning approach. *J Bridge Eng*. 2021; 26(8):04021054. doi:10.1061/(ASCE)BE.1943-5592.0001744.